Electronic Supplementary Material (ESI) for Chemical Science.

Lilypad aggregation: localised self-assembly and metal sequestration at a liquid-vapour interface

Christopher D. Jones, Aled R. Lewis, Daniel R. Jones, Christopher J. Ottley, Kaiqiang Liu and Jonathan W. Steed*

Supplementary Data

Contents:

1. Optical microscopy 1
2. Derivations
   - 2.1 Model of aggregate growth 4
   - 2.2 Total energy 5
   - 2.3 Changes in shape and volume 7
   - 2.4 Allowed surface energies 9
   - 2.5 Initial aggregate geometry 10
   - 2.6 Final aggregate geometry if $\gamma_{vap} > 0$ 10
   - 2.7 Final aggregate geometry if $\gamma_{vap} < 0$ 11
   - 2.8 Evaluation of aggregate properties 13
3. Surface energy measurements 17
4. Criteria for lilypad aggregation
   - 4.1 Aggregation tests 18
   - 4.2 Conformational analysis 20
5. Infrared spectroscopy 22
6. X-ray photoelectron spectroscopy 23
7. Scanning electron microscopy 25
8. Powder X-ray diffraction 27
9. Inductively coupled plasma mass spectrometry 28

1. Optical microscopy

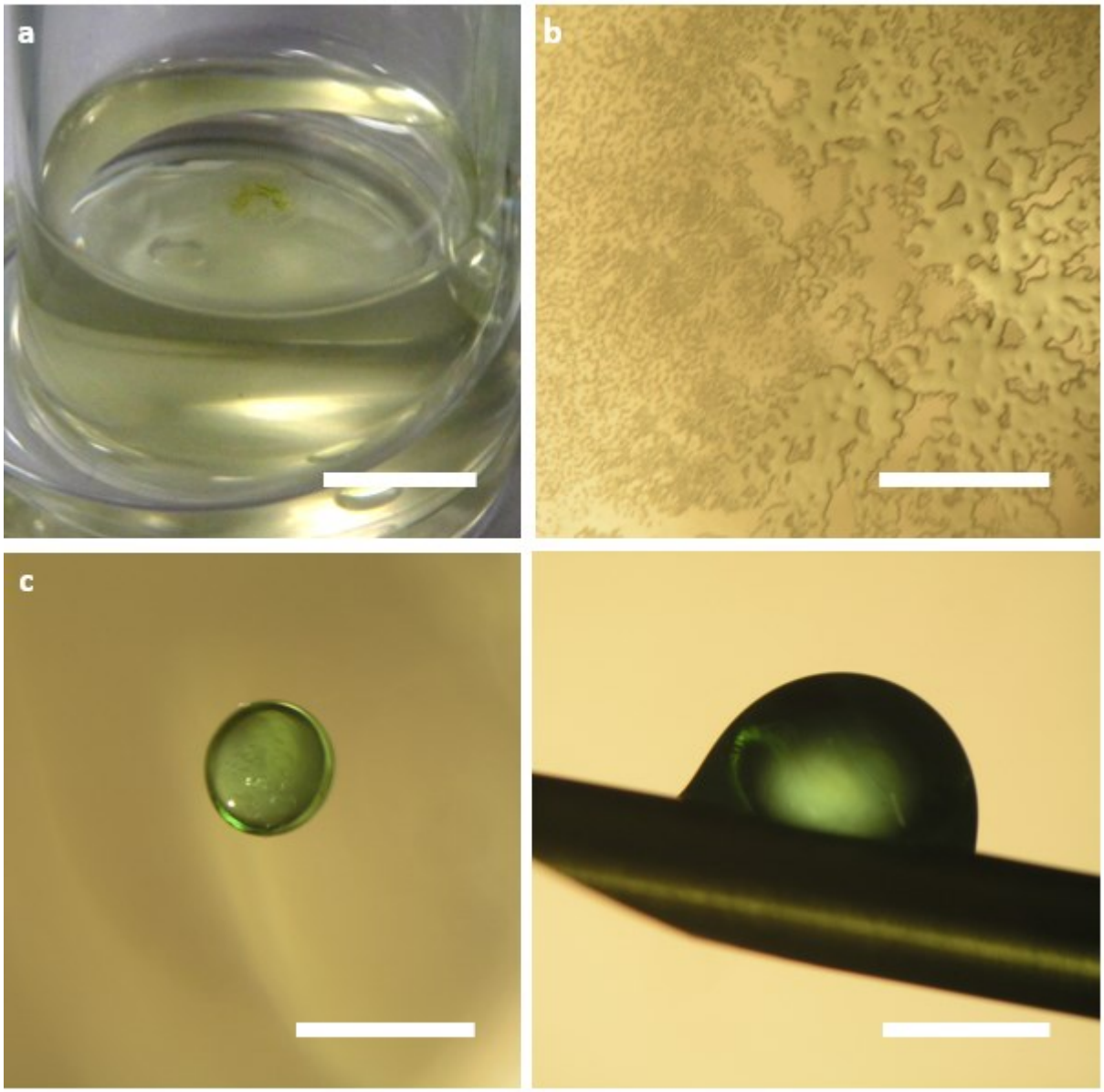

Fig. S1 Lilypad aggregates formed by the diffusion of diethyl ether vapour into a DMF solution of nickel(II) chloride hexahydrate (0.24% w/v, 10 mM) and **2** (0.20% w/v, 2.5 mM) at room temperature. A membrane of colloidal particles is visible in a photograph (a) and optical micrograph (b) of the growing aggregate after 2 hours. Micrographs of the aggregate at the sol surface (c) and upon harvesting (d) after 8 hours reveal a final interfacial radius of approximately 0.37 mm and volume of 0.15 mm^3. Scale bars (a) 5 mm, (b) 1 mm, (c) 1 mm and (d) 0.5 mm.

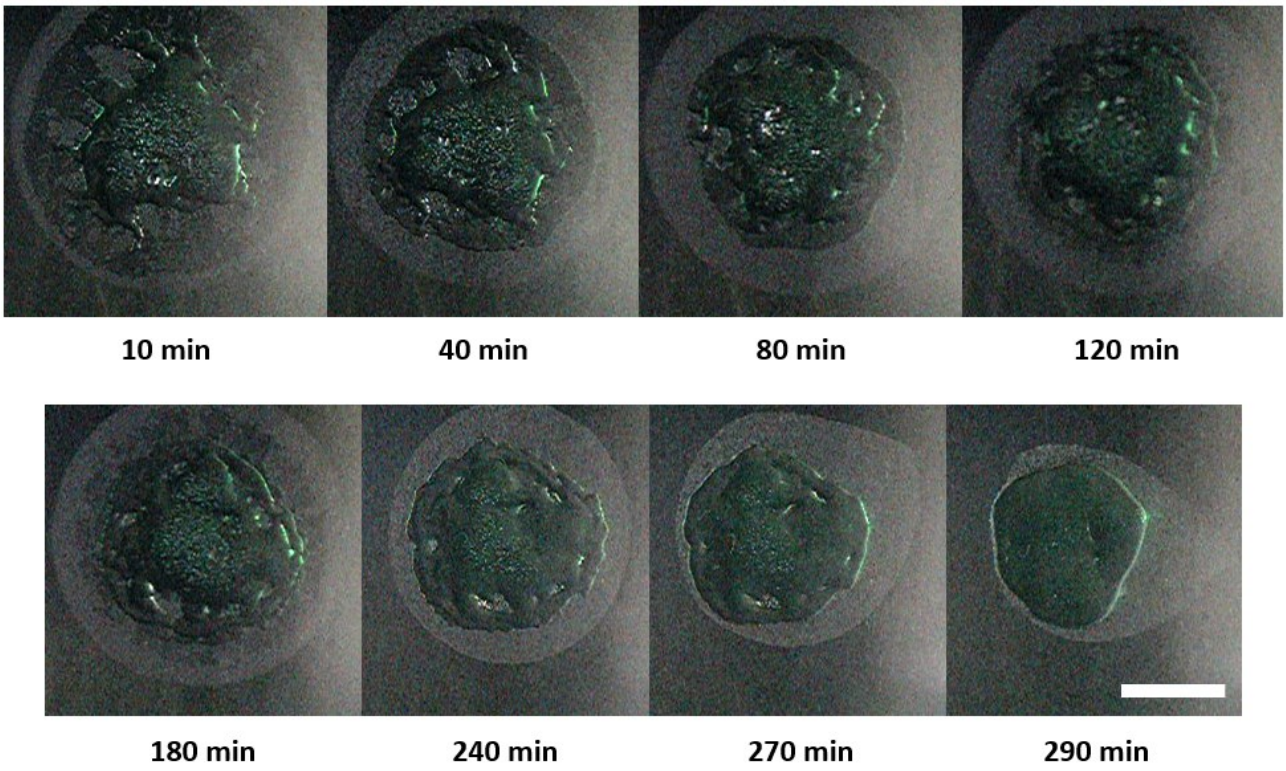

Fig. S2 Selected frames from a video of lilypad aggregate growth over 5 hours. The aggregate was prepared by the diffusion of diethyl ether vapour into a DMF solution of nickel(II) chloride hexahydrate (0.24% w/v, 10 mM) and **1** (0.50% w/v, 9.8 mM). All images were obtained at the same magnification. Scale bar 2 mm.

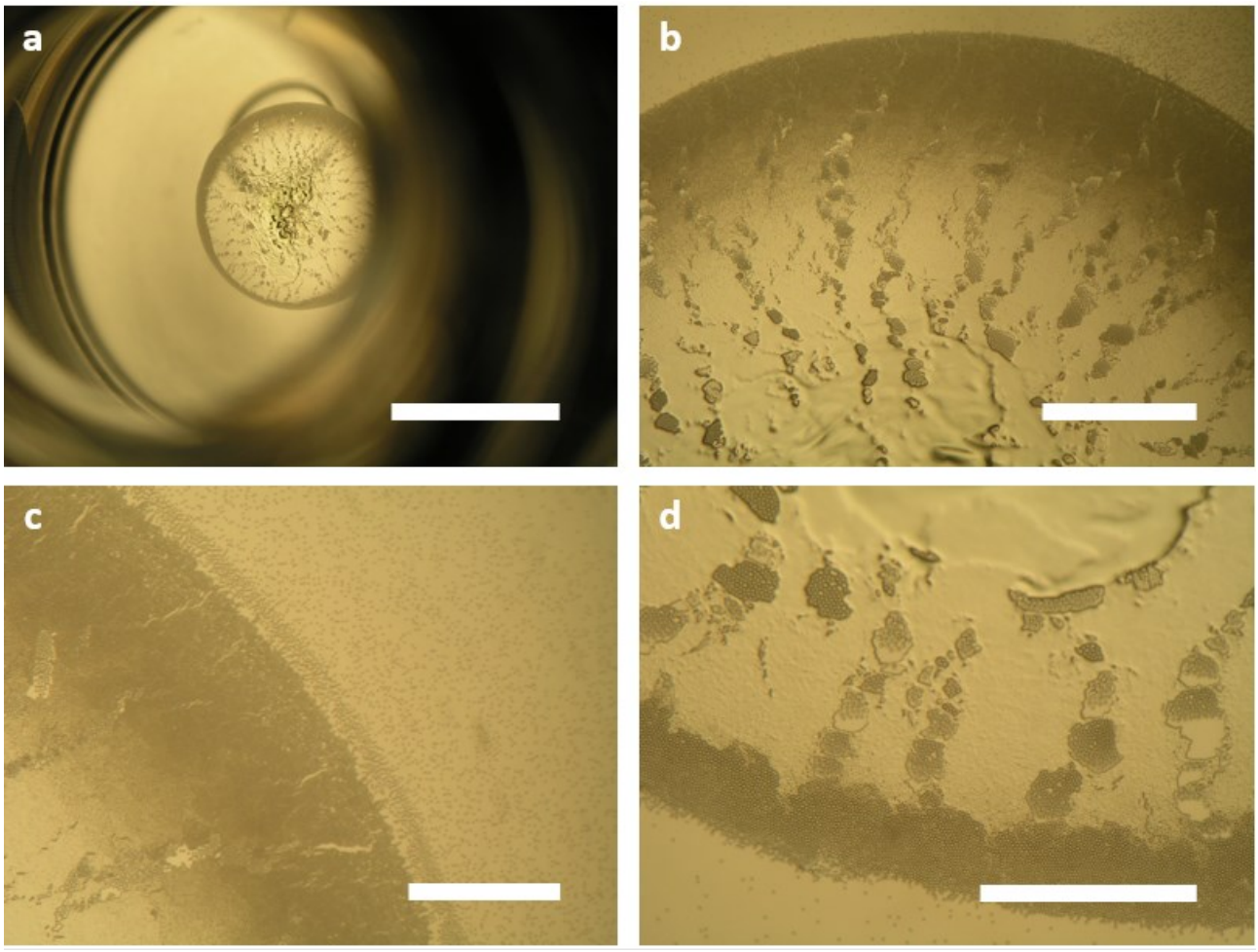

Fig. S3 Micrographs illustrating the self-assembly of colloidal particles during lilypad aggregate growth. Aggregates were prepared by the diffusion of diethyl ether vapour into a DMF solution of nickel(II) chloride hexahydrate (0.24% w/v, 10 mM) and **1** (0.50% w/v, 9.8 mM). Scale bars (a) 5 mm , (b) 1 mm and (c,d) 500 µm.

2. Derivations

2.1 Model of aggregate growth

Lilypad aggregates are observed to adopt spheroidal morphologies and do not undergo significant stretching for the majority of their growth. Thus, such an aggregate may be modelled as a spherical cap, representing a fraction of a sphere of radius R (Fig. S4). The width of the vial is much greater than both the depth of the meniscus and the diameter of the material, so the aggregate-vapour interface may be approximated by a planar interface at a minimum distance fR from the centre of the sphere. In this model, the limits $f = +1$ and -1 correspond to the cases of a spherical aggregate or no aggregate respectively.

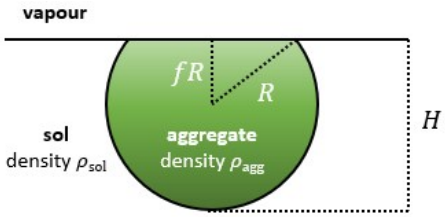

Fig. S4 Geometric model of a lilypad aggregate.

For a spherical cap of height H, the volume V is given by:

$$V = \frac{1}{3}\pi H^2(3R - H)$$

For the aggregate, $H = R(1 + f)$. Thus:

$$V = \frac{1}{3}\pi(1 + f)^2R^2(3R - R(1 + f))$$

$$= \frac{1}{3}\pi R^3\left(2 + 3f - f^3\right)$$

$$= \frac{1}{3}\pi R^3(2 - f)(1 + f)^2$$

By Pythagoras' theorem, the radius of the circular intersection between the sphere and the interface is $\sqrt{R^2 - (fR)^2} = R\sqrt{1 + f^2}$. Thus, the area of the aggregate at the interface, A_{vap}, may be expressed:

$$A_{vap} = \pi R^2(1 - f^2)$$

The area of the aggregate-sol interface, A_{sol}, is given by:

$$A_{sol} = 2\pi RH = 2\pi R^2(1 + f)$$

2.2 Total energy

The total energy of the system, E, is equal to the sum of the gravitational potential energy, E_g, and the surface energies of the aggregate-vapour and aggregate-sol interfaces, E_{vap} and E_{sol} respectively. In order to evaluate E_g, it is necessary to sum over the contributions of mass elements at a vertical distance z from the centre of the sphere:

$$E_g^{'} = g(\rho_{agg} - \rho_{sol}) \int_{-R}^{fR} \int_{0}^{2\pi} \int_{0}^{\sqrt{R^2 - z^2}} zr dr d\theta dz$$

$$= \pi g(\rho_{agg} - \rho_{sol}) \int_{-R}^{fR} z(R^2 - z^2) dz$$

$$= \pi g(\rho_{agg} - \rho_{sol}) \left[\frac{z^2}{2} \left(R^2 - \frac{z^2}{2} \right) \right]_{-R}^{fR}$$

$$= \frac{\pi g R^4}{4} (\rho_{agg} - \rho_{sol})(2f^2 - f^4 - 1)$$

Here, g is the acceleration due to gravity and ρ_{agg} and ρ_{sol} the densities of the aggregate and sol, respectively. Note that $\rho_{agg} > \rho_{sol}$ and it is assumed that neither value varies with respect to z. This is approximately true if the range in z is much smaller than the distance diffused by the antisolvent over the course of aggregate growth. However, accuracy could be improved by measuring the variation in ρ_{sol} with z and incorporating this function into the integral expression.

The coordinates of the system must be displaced to produce a fixed gravitational potential energy of zero at the aggregate-vapour interface ($z = fR$):

$$E_g = E_g^{'} - fg\rho RV$$

$$= \frac{\pi g \rho R^4}{4}\left(2f^2 - f^4 - 1\right) - \frac{\pi g \rho R^4}{3}\left(2f + 3f^2 - f^4\right)$$

$$= \frac{\pi g \rho R^4}{12}\left(-8f - 6f^2 + f^4 - 3\right)$$

$$= \frac{\pi g \rho R^4}{12}(f - 3)(1 + f)^3$$

where $\rho = (\rho_{agg} - \rho_{sol})$. If γ_{vap} and γ_{sol} are the surface energies of the aggregate-vapour and aggregate-sol interfaces respectively, the total energy E is expressed:

$$E = E_g + \gamma_{vap} A_{vap} + \gamma_{sol} A_{sol}$$

$$E = \frac{\pi g \rho R^4}{12}(f - 3)(f + 1)^3 + \pi R^2 (1 + f)\left(\gamma_{vap}(1 - f) + 2\gamma_{sol}\right) \qquad (1)$$

It should be noted that creation of a aggregate-vapour reduces the area of the sol-vapour interface by an area A_{vap}. Thus, the energy of the sol-vapour interface is incorporated into the value γ_{vap}. Furthermore, since both γ_{sol} and γ_{vap} represent differences between the interactions of the aggregate and sol, the values of these parameters are likely to be small.

For a stable aggregate with realistic values of ρ, γ_{vap} and γ_{sol}, the combined surface energy terms are much larger than E_g for most values of f and V (Fig. S5). It is therefore reasonable to assume the aggregate adopts an approximate spherical cap morphology in order to minimise unfavourable surface energy contributions. At constant V, a local minimum is produced only by the term in γ_{sol} (Fig. S5a,b). Thus, it is this term that is responsible for the feasibility of lilypad aggregation. The term in γ_{sol} increases dramatically as the aggregate grows, counterbalancing a comparable increase in the magnitude of E_g (Fig. S5c,d). By contrast, the term in γ_{vap} remains small and plateaus with increasing V, eventually decreasing in magnitude near the completion of aggregate growth. It may be concluded that the aggregate-vapour interface increases stability mainly by reducing the area of the aggregate-sol boundary, and aggregate-vapour interactions are directly important only in the early stages of aggregation.

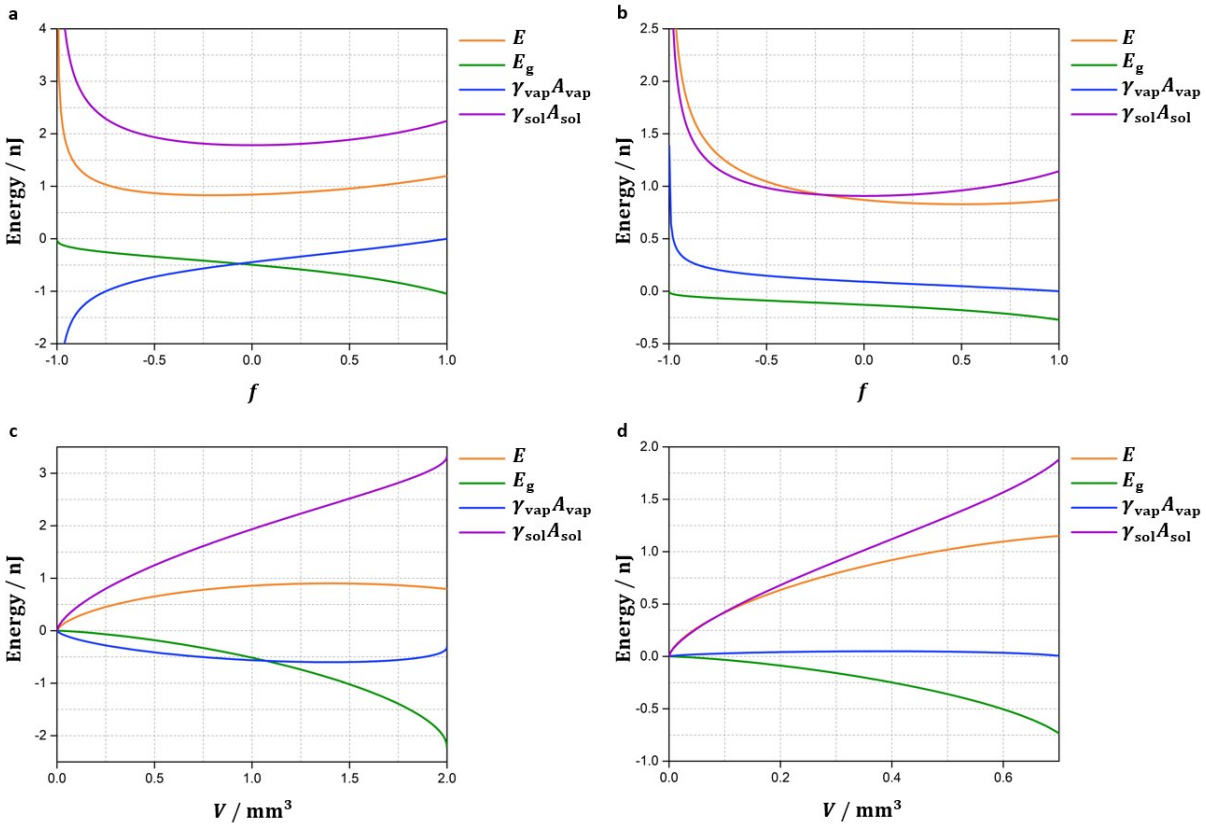

Fig. S5 (a) Surface energy, gravitational energy and total energy functions for a lilypad aggregate of varying f and constant $V = 0.90\ mm^3$, with $g = 9.81\ m\ s^{-2}$, $\rho = 200\ kg\ m^{-3}$, $\gamma_{vap} = -0.25\ mJ\ m^{-2}$ and $\gamma_{sol} = +0.50\ mJ\ m^{-2}$. The minimum value of E indicates the morphology at which the aggregate is most stable, and occurs at $f = -0.2$ for these parameters; (b) energies for an aggregate of varying f and constant $V = 0.90\ mm^3$, with $\gamma_{vap} = +0.10\ mJ\ m^{-2}$ and $\gamma_{sol} = +0.50\ mJ\ m^{-2}$ and a minimum at $f = +0.5$; (c) energies of a growing aggregate with with $\gamma_{vap} = -0.25\ mJ\ m^{-2}$ and $\gamma_{sol} = +0.50\ mJ\ m^{-2}$, where the aggregate adopts the most stable value of f at each value of V; (d) energies of a growing aggregate with with $\gamma_{vap} = +0.10\ mJ\ m^{-2}$ and $\gamma_{sol} = -0.50\ mJ\ m^{-2}$.

2.3 Changes in shape and volume

The aggregate adopts its most stable morphology when the value of f produces a local minimum in E. Thus, to determine the optimal value of f for a given aggregate mass, E is differentiated with respect to f at constant V and set to zero:

$$\left(\frac{\partial E}{\partial f}\right)_V = \pi R\left(\frac{\partial R}{\partial f}\right)_V\left(\frac{g\rho R^2}{3}(f-3)(f+1)^3 + 2(1+f)\left(\gamma_{vap}(1-f)+2\gamma_{sol}\right)\right) + \pi$$
$$= 0$$

Substituting the expression for V and noting that $R \neq 0$:

$$\left(\frac{\partial R}{\partial f}\right)_V(1+f)\left(\frac{g\rho R^2}{3}(f-3)(1+f)^2 + 2\left(\gamma_{vap}(1-f)+2\gamma_{sol}\right)\right) - \frac{g\rho V}{\pi} + 2R\left(\gamma_{sol} - f\gamma_{vap}\right) = 0$$

From the expression for V:

$$R = \left(\frac{3V}{\pi(2-f)(1+f)^2}\right)^{1/3}; \quad \left(\frac{\partial R}{\partial f}\right)_V = \left(\frac{3V}{\pi(2-f)^4(1+f)^5}\right)^{1/3}(f-1)$$

Thus:

$$\left(\frac{3V}{\pi(2-f)^4(1+f)^2}\right)^{1/3}(f-1)\left(\frac{g\rho}{3}\left(\frac{3V}{\pi(2-f)(1+f)^2}\right)^{2/3}(f-3)(1+f)^2 + 2\left(\gamma_{vap}(1-f)+2\gamma_{sol}\right)\right) - \frac{g\rho V}{\pi} + 2$$
$$\left(\frac{3V}{\pi(2-f)(1+f)^2}\right)^{1/3}\left(\gamma_{sol} - f\gamma_{vap}\right) = 0$$

Setting $a = (2-f)(1+f)^2$:

$$\left(\frac{3V}{\pi a}\right)^{1/3}\frac{f-1}{2-f}\left(\frac{g\rho}{3}\left(\frac{3V}{\pi a}\right)^{2/3}(f-3)(1+f)^2 + 2\left(\gamma_{vap}(1-f)+2\gamma_{sol}\right)\right) - \frac{g\rho V}{\pi} + 2\left(\frac{3V}{\pi a}\right)^{1/3}$$
$$\left(\gamma_{sol} - f\gamma_{vap}\right) = 0$$

Simplifying and collecting terms:

$$\frac{(f-1)}{(2-f)^2}\left(g\rho(f-3)\left(\frac{aV^2}{3\pi^2}\right)^{1/3} + 2(2-f)\left(\gamma_{vap}(1-f)+2\gamma_{sol}\right)\right) - g\rho\left(\frac{aV^2}{3\pi^2}\right)^{1/3} + 2\left(\gamma_{sol} - f\gamma_{vap}\right)$$
$$= 0$$

$$bV^{\frac{2}{3}}\left(\frac{(f-1)(f-3)}{(2-f)^2} - 1\right) = \left(4\left(\frac{1-f}{2-f}\right) - 2\right)\gamma_{sol} + \left(2\frac{(1-f)^2}{2-f} + 2f\right)\gamma_{vap}$$

where $b = g\rho\left(\frac{a}{3\pi^2}\right)^{1/3}$. Solving for V:

$$bV^{\frac{2}{3}}\left(\frac{f^2-4f+3-4+4f-f^2}{(2-f)^2}\right)=\left(\frac{4-4f-4+2f}{2-f}\right)\gamma_{sol}+\left(\frac{2-4f+2f^2+4f-2f^2}{2-f}\right)\gamma_{vap}$$

$$bV^{\frac{2}{3}}\left(\frac{-1}{2-f}\right)=-2f\gamma_{sol}+2\gamma_{vap}$$

$$V=2\sqrt{6}\pi\left(\frac{2-f}{1+f}\right)\left(\frac{f\gamma_{sol}-\gamma_{vap}}{\rho g}\right)^{3/2} \qquad (2)$$

If $\gamma_{vap}<0$, some values of V return two possible solutions for f. In all cases, the least positive value of f always corresponds to the local minimum in $E(f)$. The second solution corresponds to a local maximum in $E(f)$ so does not represent an equilibrium geometry.

The value of V increases as γ_{sol} becomes more positive and γ_{vap} more negative. This is intuitively reasonable: larger aggregates may be supported if they are more strongly attracted to the aggregate-vapour interface, and more strongly repelled by the surrounding sol.

2.4 Allowed surface energies

Rearranging equation (2) reveals a linear relationship between γ_{vap} and γ_{sol}:

$$\gamma_{vap}=f\gamma_{sol}-\frac{\rho g}{2}\left(\frac{1}{\sqrt{3}\pi}\left(\frac{1+f}{2-f}\right)V\right)^{2/3}=f\gamma_{sol}+c \qquad (3)$$

Physical solutions $V>0$ are possible if and only if $\gamma_{vap}<f\gamma_{sol}$. Likewise, $-1<f<1$ for an aggregate with non-zero volume and a non-zero area at the aggregate-vapour interface. If an aggregate drops when it is fully spherical, $f\to1$ and $\gamma_{vap}<\gamma_{sol}$. At the beginning of aggregate growth, $V\to0$ and the inequality $f\to f_{start}>-1$ must hold, such that

$$\left(\frac{\gamma_{vap}}{\gamma_{sol}}\right)\to f_{start}>-1$$

Thus $\gamma_{vap}>-\gamma_{sol}$. Combining these observations, it may be concluded that $\gamma_{sol}>0$ for all f: lilypad aggregation cannot occur if the aggregate-sol interface displays a negative surface energy. The

energy of the aggregate-vapour interface can be positive or negative, but must not be greater in magnitude than γ_{sol}. The allowed values of $(\gamma_{sol},\gamma_{vap})$ occupy one quadrant in a plot of γ_{vap} against γ_{sol}, bounded by the lines $\gamma_{vap} = \gamma_{sol}$ and $\gamma_{vap} = -\gamma_{sol}$ (Fig. S6).

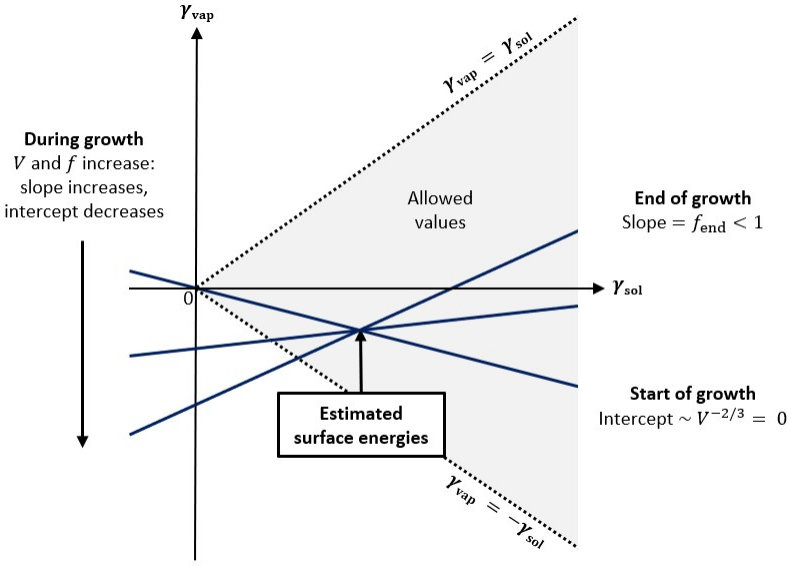

Fig. S6 Schematic plot of γ_{vap} against γ_{sol}, illustrating the method by which the geometry of a lilypad aggregate is used to estimate its surface energies.

For a given value of V with constant ρg, a straight line in the plot intersects all combinations $(\gamma_{sol},\gamma_{vap})$ that will produce aggregates of identical shape. The shape is specified by the value f, given by the gradient of the line, while *V* may be determined from the intercept value.

2.5 Initial aggregate geometry

The shape of the aggregate at the beginning of growth is indicated by the slope, f_{start}, of the line connecting $(\gamma_{sol},\gamma_{vap})$ with the origin. This parameter is given by the ratio of the two surface energies:

$$f_{start} = \frac{\gamma_{vap}}{\gamma_{sol}}$$

2.6 Final aggregate geometry if $\gamma_{vap} > 0$

If $\gamma_{vap} > 0$, increasing f always produces a stable morphology with a larger value of V (Fig. S7a). The minimum in $E(f)$ is the only turning point corresponding to a physical value of V, so $V(f)$ can be evaluated directly from equation (1). The minimum at $f = 1$, $V(1)$, is equal to the maximum volume

of the aggregate at the point of dropping, V_{end}. This value can be calculated from the intercept of the line which has slope $f = 1$ and intersects the point $(\gamma_{sol}, \gamma_{vap})$:

$$V_{end} = V(1) = \sqrt{6}\pi\left(\frac{\gamma_{sol} - \gamma_{vap}}{\rho g}\right)^{3/2}$$

If $\gamma_{vap} > 0$, the aggregate is always fully spherical when the volume is maximised ($f_{end} = 1$).

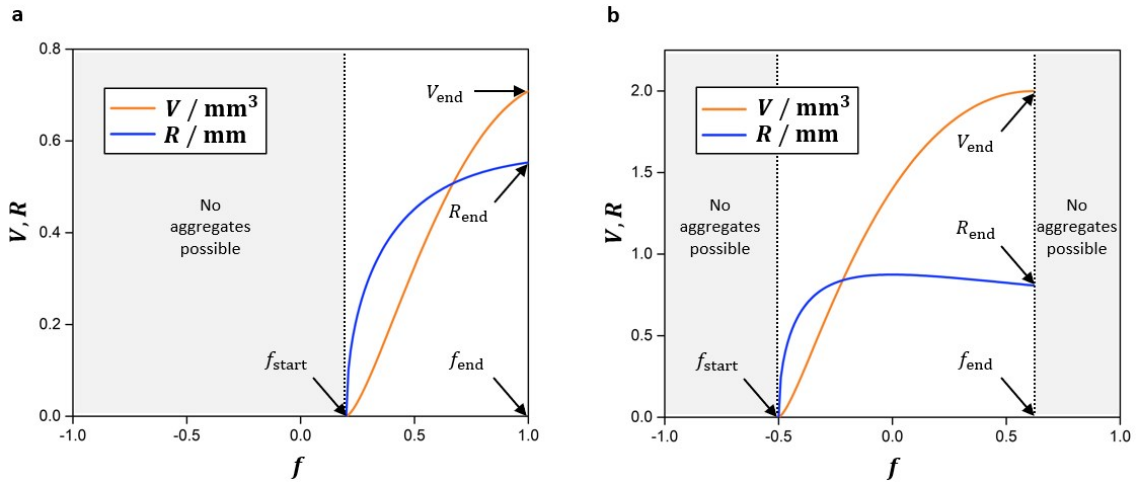

Fig. S7 Variation of V with f for growing aggregates, where $\gamma_{sol} = +0.50\ mJ\ m^{-2}$ and (b) $\gamma_{vap} = +0.10\ mJ\ m^{-2}$ or (a) $-0.25\ mJ\ m^{-2}$. For each value of V, the aggregates adopt the value of f at which E is minimised. The final value of f, f_{end}, is the value of f at which V is maximised. Note that $f_{end} = 1$ if $\gamma_{vap} > 0$ and $f_{end} < 1$ if $\gamma_{vap} < 0$.

2.7 Final aggregate geometry if $\gamma_{vap} < 0$

If $\gamma_{vap} < 0$, V_{end} is significantly greater than $V(1)$ (Fig. S7b), and the function $E(f)$ may contain a local maximum in addition to a minimum (Fig. S8). As the aggregate grows, the most stable value of f approaches f_{end}, and the maximum and minimum are replaced by a point of inflexion. Further growth of the aggregate is not possible, as $E(f)$ displays no local minimum for all $V(f) > V_{end}$: there is no value of f for which aggregates larger than V_{end} are stable at the interface. It should be noted that for some values of $V > V_{end}$, equation (2) may be satisfied by a value $f > f_{end}$. This value corresponds to the local maximum in $E(f)$ and does not represent an equilibrium geometry.

Because $f_{end} < 1$ at the end of aggregate growth, the material does not form a complete sphere before sinking occurs. This phenomenon is analogous to flocculation: the value of f at the local minimum is not necessarily the lowest energy morphology, but the system is inhibited from reaching

$f = 1$ by an activation barrier E_a. As V increases, E_a decreases and the aggregate becomes less stable at the interface. The minimum in $E(f)$, representing the most stable aggregate morphology, shifts to a higher value of f, and the position of the maximum in $E(f)$ decreases proportionally. When V_{end} is reached, the minimum and maximum converge at $f = f_{end}$, such that $E_a = 0$ and the aggregate spontaneously sinks. It should be noted that V is often smaller than V_{end} at the point of sinking, as the small magnitude of E_a in the region of V_{end} means that the system is sensitive to even minor perturbations.

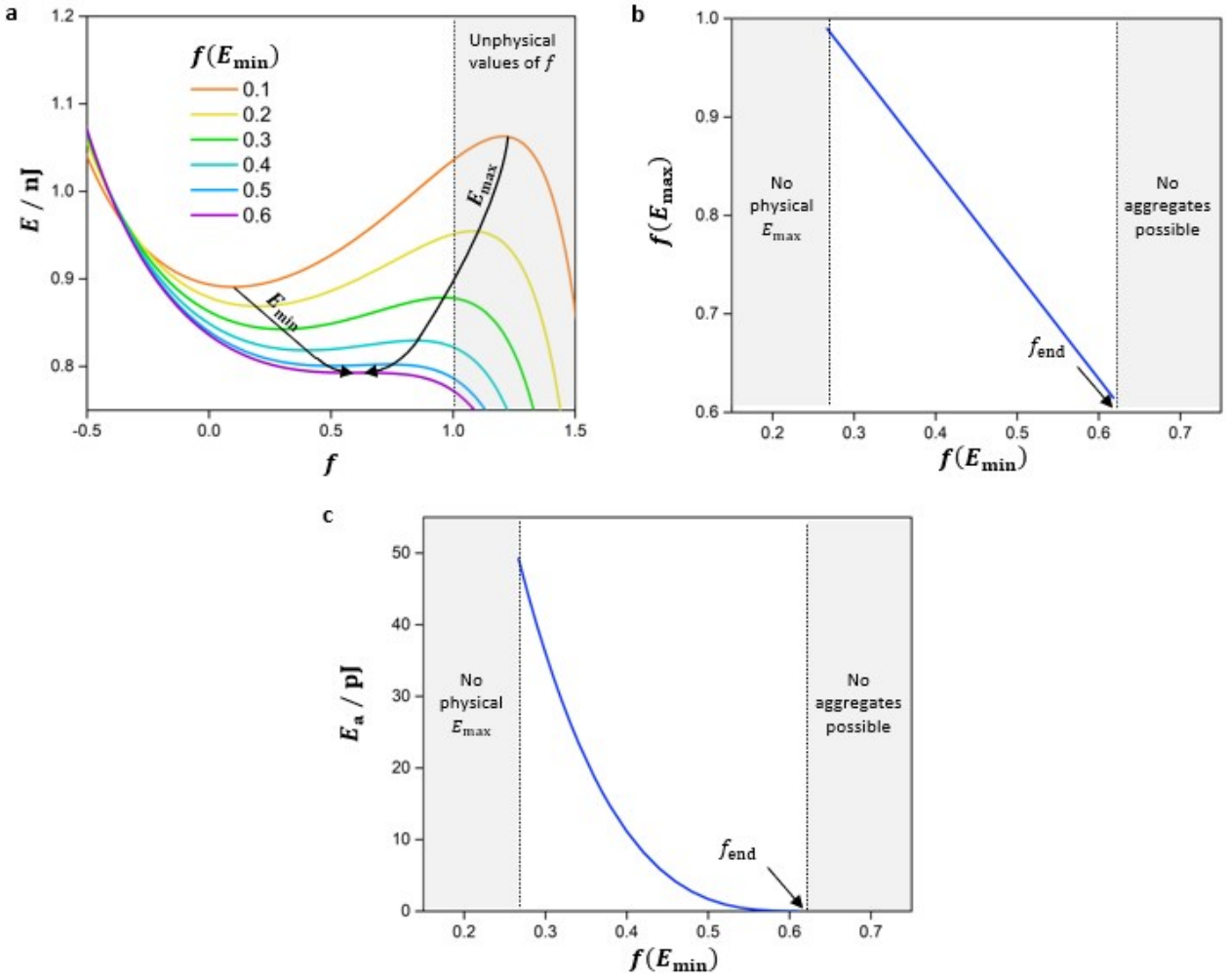

Fig. S8 (a) Potential energy plots for a growing aggregate with $g = 9.81\ m\ s^{-2}$, $\rho = 200\ kg\ m^{-3}$, $\gamma_{vap} = -0.25\ mJ\ m^{-2}$ and $\gamma_{sol} = 0.50\ mJ\ m^{-2}$. At each stage of growth, the aggregate adopts the value of f corresponding to the local minimum in $E(f)$, E_{min}. (b) Positions of the local maximum energy, E_{max}, at varying values of f. This position, $f(E_{max})$, decreases in linear proportion to f, and the two values become equal when $V = V_{end}$. Note that unphysical values $f(E_{max}) > 1$ may occur for small aggregates. (c) Values of $E_a = E_{max} - E_{min}$ for a growing aggregate. Sinking of the aggregate can occur for all physical values of E_{max}, and E_a represents the activation barrier

for this process. As V approaches V_{end}, the activation barrier E_a decreases, making sinking more likely. In this example, $f_{end} = 0.62$ and $V_{end} = 2.0\ mm^3$.

The value of V_{end} is determined by maximising V with respect to f:

$$\frac{\partial V}{\partial f} = 2\sqrt{6}\pi\left(\left(\frac{-1}{1+f} - \frac{2-f}{(1+f)^2}\right)\left(\frac{f\gamma_{sol} - \gamma_{vap}}{\rho g}\right)^{3/2} + \frac{3\gamma_{sol}}{2\rho g}\left(\frac{2-f}{1+f}\right)\left(\frac{f\gamma_{sol} - \gamma_{vap}}{\rho g}\right)^{1/2}\right) = 0$$

The solution $f\gamma_{sol} - \gamma_{vap} = 0$ corresponds to the trivial case $V = 0$. For the other solutions:

$$f(1+f)\gamma_{sol} - 2(\gamma_{sol} + \gamma_{vap}) = 0$$

Thus:

$$f = \frac{1}{2}\left(-1 \pm \sqrt{9 + 8\frac{\gamma_{vap}}{\gamma_{sol}}}\right)$$

The negative root in this expression returns an unphysical value $f < -1$ for all possible negative ratios of γ_{vap} and γ_{sol}, so f_{end} must correspond to the other solution:

$$f_{end} = \frac{1}{2}\left(-1 + \sqrt{9 + 8\frac{\gamma_{vap}}{\gamma_{sol}}}\right) \qquad (4)$$

For all aggregates, $f_{end} > 0$. The aggregate is stable at the interface at least until it is half-spherical in shape.

Substituting the expression into (3):

$$V_{end}(\gamma_{vap} < 0) = \frac{\sqrt{3}\pi}{4}\left(\frac{3\sqrt{9 + 8\frac{\gamma_{vap}}{\gamma_{sol}}} - 4\frac{\gamma_{vap}}{\gamma_{sol}} - 7}{\frac{\gamma_{vap}}{\gamma_{sol}} + 1}\right)\left(\frac{\gamma_{sol}\sqrt{9 + 8\frac{\gamma_{vap}}{\gamma_{sol}}} - 2\gamma_{vap} - \gamma_{sol}}{\rho g}\right)^{3/2}$$

If $\gamma_{vap} = 0$, the expressions for V_{end} at $\gamma_{vap} < 0$ and $\gamma_{vap} < 0$ produce identical values, as required.

$$V_{end}(\gamma_{vap} = 0) = \frac{\sqrt{3}\pi}{4}\left(\frac{3\sqrt{9} - 7}{1}\right)\left(\frac{\gamma_{sol}\sqrt{9} - \gamma_{sol}}{\rho g}\right)^{\frac{3}{2}} = \frac{\sqrt{3}\pi}{4}(2)\left(\frac{2\gamma_{sol}}{\rho g}\right)^{\frac{3}{2}} = \sqrt{6}\pi\left(\frac{\gamma_{sol}}{\rho g}\right)^{\frac{3}{2}}$$

2.8 Evaluation of aggregate properties

The growth profile of the aggregate at fixed values of γ_{vap} and γ_{sol} can be evaluated by drawing lines of increasing gradient through the point $(\gamma_{sol},\gamma_{vap})$. The first physical value of f, f_{start}, corresponds to the gradient of the straight line that intersects both $(\gamma_{sol},\gamma_{vap})$ and the origin. For $\gamma_{vap} > 0$, all lines with gradients larger than f_{start} correspond to energetically accessible morphologies. For $\gamma_{vap} < 0$, however, lines with gradients above f_{end} do not correspond to real stages in the aggregate growth profile.

Unknown values of γ_{vap} and γ_{sol} may be estimated by measuring *f* and *V* at each stage of aggregate growth, plotting the corresponding straight lines on the surface energy plot, and identifying the points of intersection for successive lines. If there is no common point of intersection, it may be concluded that ρ, γ_{vap} and/or γ_{sol} do not remain constant throughout the experiment. Errors in the estimates of γ_{vap} and γ_{sol} may also arise if the aggregate is not a perfect spherical cap. A line is drawn for each combination of f and R values within the range of measurements, and errors are estimated by calculating the standard deviation of the points of intersection.

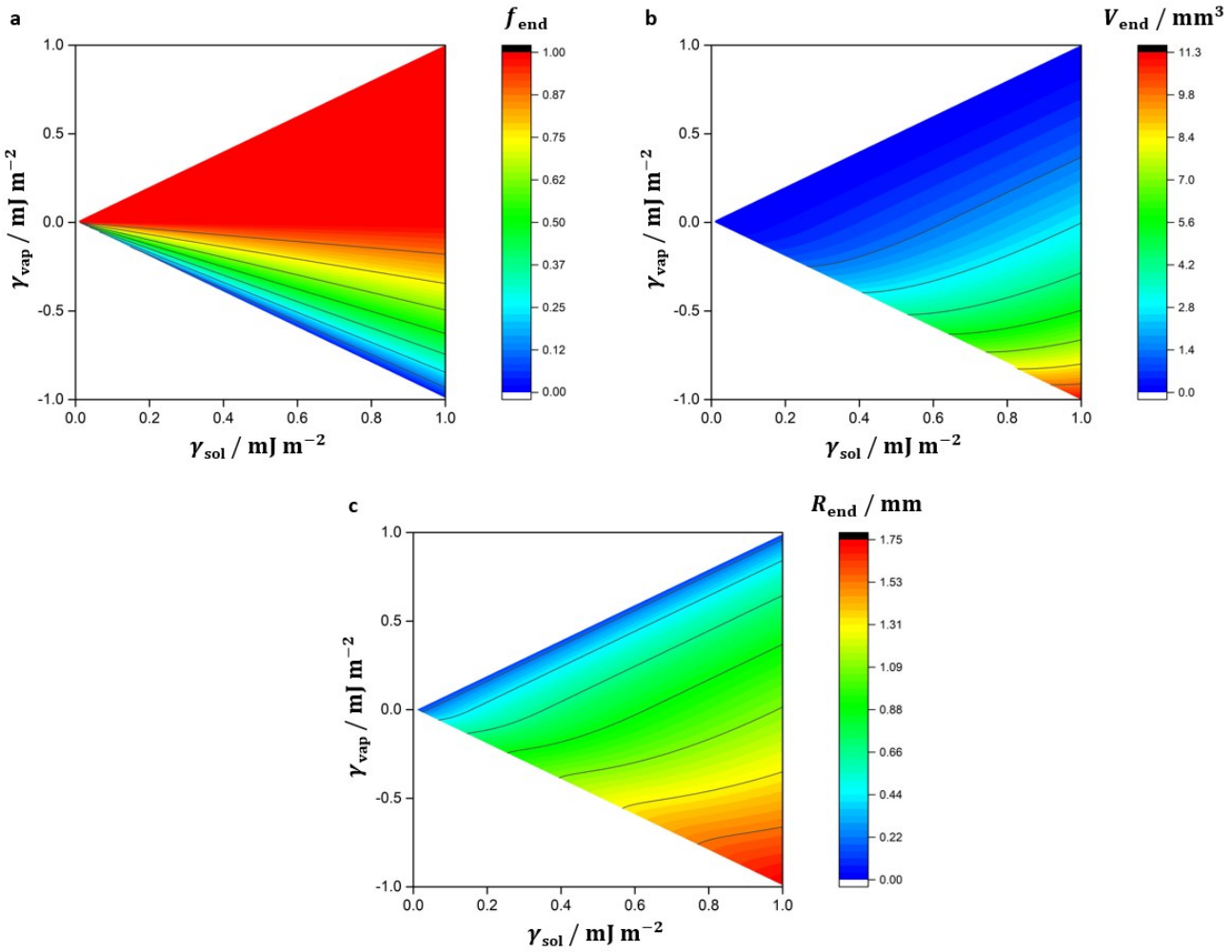

Fig. S9 Variations in (a) f_{end}, (b) V_{end} and (c) R_{end} when $g = 9.81\ m\ s^{-2}$ and $\rho = 200\ kg\ m^{-3}$. Contours indicate combinations of surface energies that generate equal geometric parameters. Note that $f_{end} > 0$ always and $f_{end} = 1.0$ exactly for all $\gamma_{vap} > 0$. More positive values of γ_{sol} and more negative values of γ_{vap} favour larger aggregates (greater V_{end} and R_{end}) with flatter morphologies (lower f_{end}).

It is interesting to note that f_{end} depends only on the ratio of the surface energies, so equation (4) applies generally to all possible physical scenarios where $\gamma_{vap} < 0$. As expected, $f_{end} = 1$ for $\gamma_{vap} = 0$ and unphysical values $f_{end} > 1$ are obtained for $\gamma_{vap} > 0$. On a plot of of γ_{vap} against γ_{sol}, combinations of surface energies with the same value of f_{end} are represented by straight lines intersecting the origin (Fig. S9a).

For realistic surface energies in the range $0 < \gamma_{vap}(mJ\ m^{-2}) < 1$, values of V_{end} are typically on the order of 1 mm^3. Coordinates of equal V_{end} are specified by curved lines in the surface energy plot (Fig. S9b). Likewise, values of V_{end} and f_{end} may be used to identify surface energies producing the

same maximum aggregate radius, R_{end} (Fig. S9c). If only the final aggregate mass, volume or radius is known, a single contour may be drawn representing all possible values of γ_{vap} and γ_{sol}. In some cases, the sign of γ_{vap} can also be confidently determined.

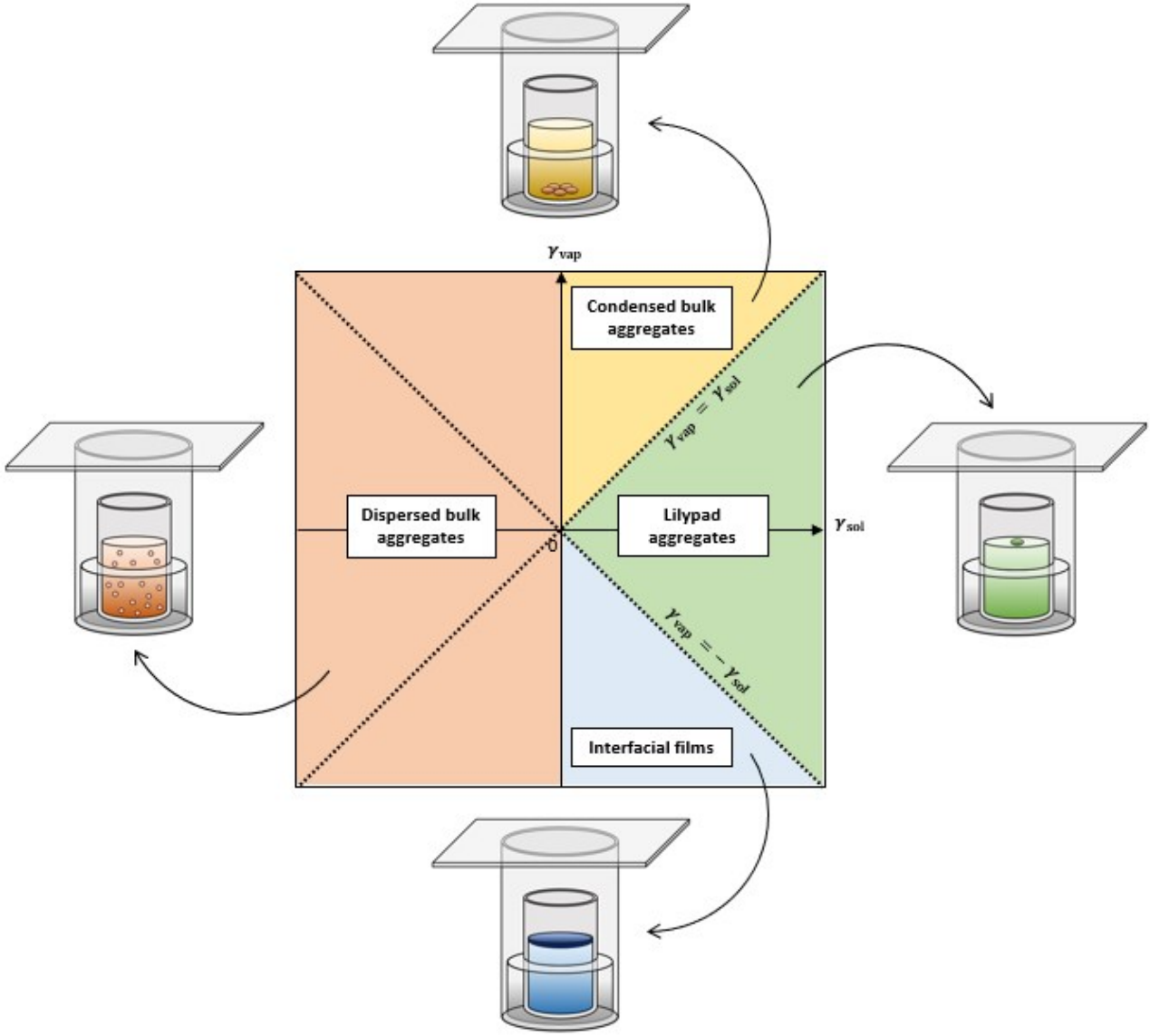

Fig. S10 Surface energy plot and schematic diagrams illustrating the expected behaviour of growing aggregates with $\rho_{agg} > \rho_{sol}$ and different combinations of γ_{sol} and γ_{vap}. If $\gamma_{sol} > 0$, lilypad aggregates are possible only if $|\gamma_{vap}| < \gamma_{sol}$. Continuous interfacial films occur if $\gamma_{vap} <- \gamma_{sol}$ and condensed bulk aggregates are formed if $\gamma_{vap} > \gamma_{sol}$. Finally, systems with $\gamma_{sol} \leq 0$ give rise to high-surface-area aggregates such as spherulites, gels and colloidal suspensions. Given that these other modes of self-assembly are frequently observed, we hypothesise that lilypad aggregation is feasible in a wide range of chemical systems.

It is instructive to consider the behaviour of aggregates with $\rho_{agg} > \rho_{sol}$ at the limiting values of γ_{sol} and γ_{vap} (Fig. S10). As noted previously (Section 2.2, Fig. S5), lilypad aggregation is possible

because a spheroid of constant V exhibits a local minimum in $\gamma_{sol}A_{sol}$ with varying f. If $\gamma_{sol} \leq 0$, interfacial structures are unstable for all values of f and aggregation takes place in the bulk of the sol. Bulk aggregation also occurs if $\gamma_{vap} > \gamma_{sol} > 0$, as such a highly unfavourable aggregate-vapour interface ensures that spherical structures ($f = 1$ and $A_{vap} = 0$) are lower in energy than all possible spherical cap morphologies. By contrast, if $\gamma_{sol} > 0$ and $\gamma_{vap} < -\gamma_{sol}$, the energy of the aggregate is minimised when the material forms a continuous interfacial film ($f \to -1$, $R \to \infty$). Although the shapes and sizes of aggregates depend on kinetic factors such as growth and nucleation rates, the structures are likely to develop such to maximise the areas of favourable interfaces. Thus, bulk aggregation in systems with $\gamma_{sol} > 0$ are expected to give rise to condensed precipitates, while materials with $\gamma_{sol} \leq 0$ may be dispersed throughout the sol as spherulites, gel networks or colloidal suspensions.

3. Surface energy measurements

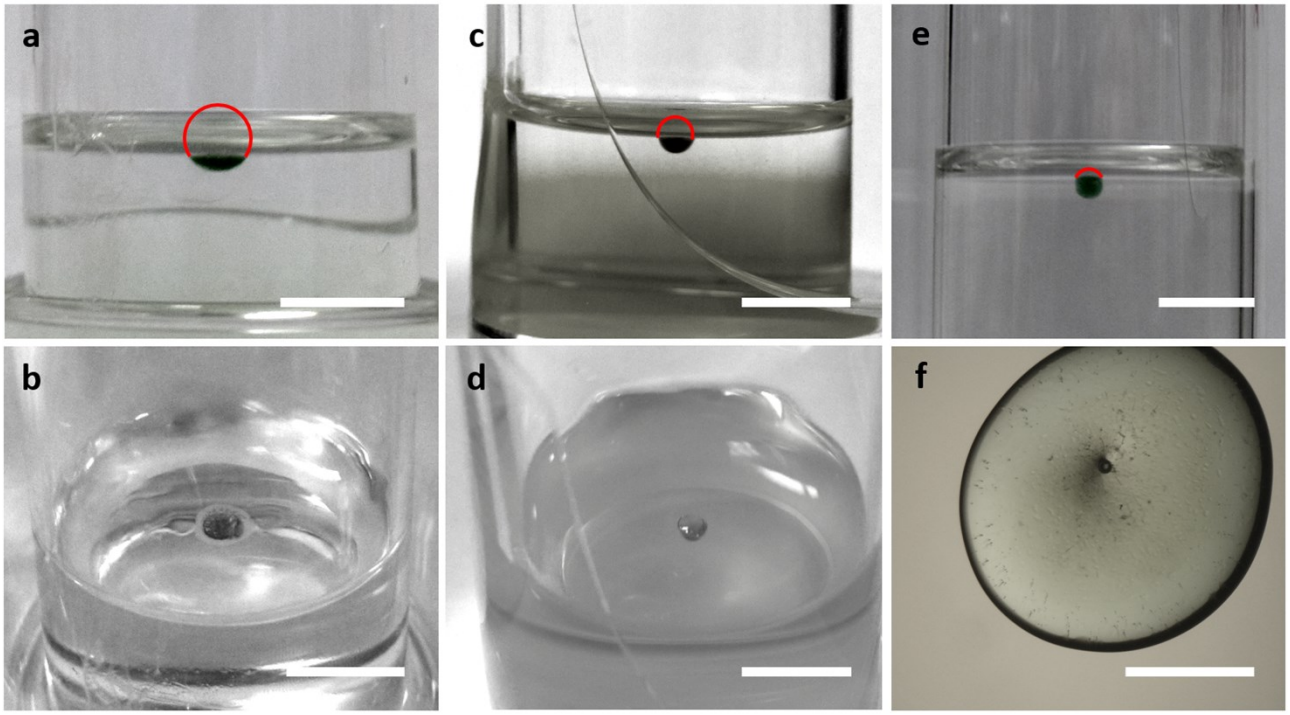

Fig. S11 Side and top-down views of lilypad aggregates where (a,b) $f = -0.66$, $R = 1.34\ mm$ and $V = 0.77\ mm^3$; (c,d) $f = -0.10$, $R = 0.81\ mm$ and $V = 0.93\ mm^3$; and (e,f) $f = 0.55$, $R = 0.72\ mm$ and $V = 1.38\ mm^3$. Scale bars of photographs (a-e) represent $5\ mm$, while scale bar for the optical micrograph (f) represents $0.5\ mm$. Aggregates represent fractions of spheres delineated in red. Images are displayed in greyscale with enhanced contrast to aid identification of the aggregate boundaries.

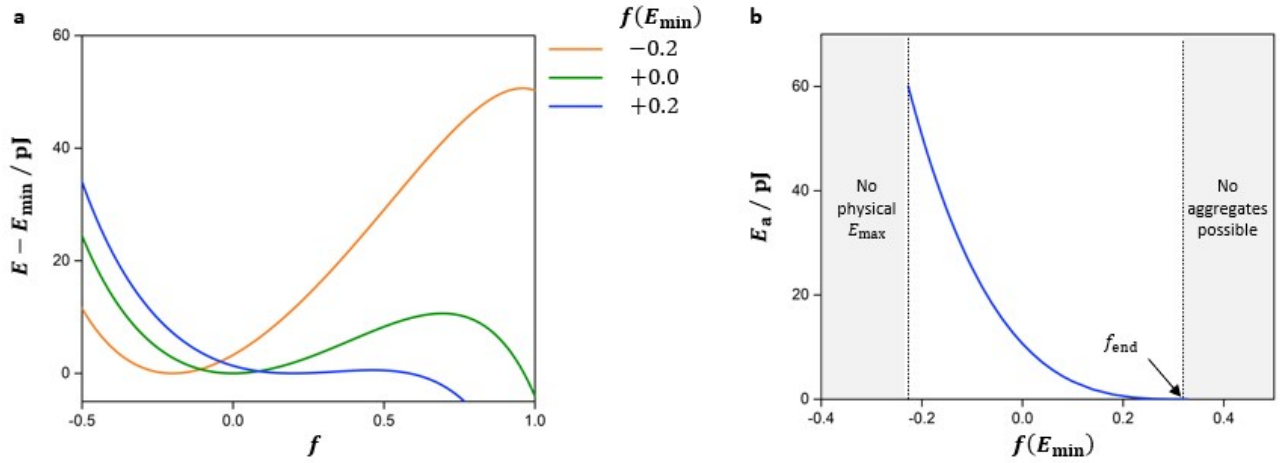

Fig. S12 (a) Potential energy profiles and (b) E_a values for typical lilypad aggregates in this study. The estimated surface energies are $\gamma_{sol} = 0.25 \pm 0.11\ mJ\ m^{-2}$ and $\gamma_{vap} = -0.20 \pm 0.07\ mJ\ m^{-2}$, and $\rho = 180 \pm 50\ kg\ m^{-3}$.

4. Criteria for lilypad aggregation

4.1 Aggregation tests

Salt	Antisolvent	Result
None	None	Solution
	Methanol	Precipitate
	Acetone	Precipitate
	Tetrahydrofuran	Precipitate
	Diethyl ether	Precipitate
$NiCl_2$·$6H_2O$	None	Solution
	Methanol	Solution, very light precipitate over 3 days
	Acetone	Solution, very light precipitate over 3 days
	Tetrahydrofuran	Light precipitate at interface
	Diethyl ether	**Lilypad aggregate**
$CoCl_2$·$6H_2O$	None	Solution
	Methanol	Solution, very light precipitate over 3 days
	Acetone	Light precipitate at interface
	Tetrahydrofuran	Light precipitate at interface
	Diethyl ether	Light precipitate at interface
$CuCl_2$·$2H_2O$	None	Solution
	Methanol	Precipitate at interface
	Acetone	Precipitate at interface
	Tetrahydrofuran	Precipitate at interface
	Diethyl ether	Precipitate at interface
$ZnCl_2$	None	Solution
	Methanol	Solution, very light precipitate over 3 days
	Acetone	Precipitate at interface
	Tetrahydrofuran	Precipitate at interface
	Diethyl ether	Precipitate at interface

Table S1 Results of aggregation experiments with different antisolvents and chloride salts. Vapour of the antisolvent was diffused at room temperature into a DMF solution of **1** (0.50% w/v, 9.8 mM) and the chloride salt (10 mM, 1 eq.). Observations were made after 8 hours unless otherwise stated.

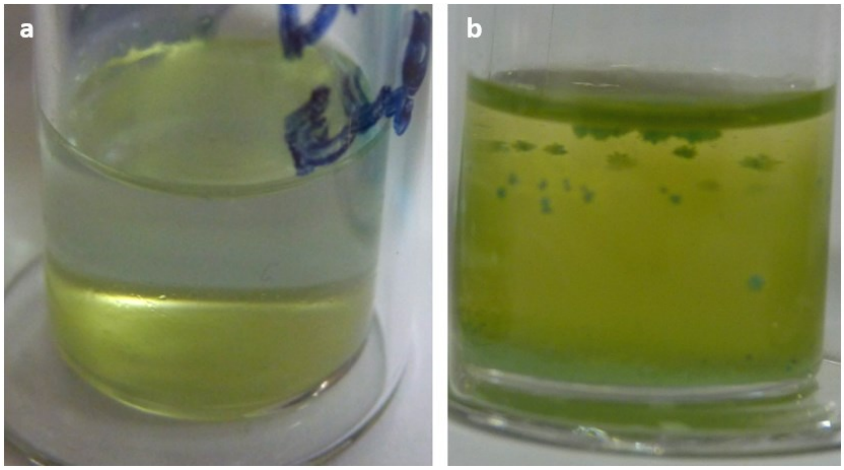

Fig. S13 Aggregates formed by diffusion of diethyl ether vapour into (a) a dimethylacetamide solution of **1** (0.50% w/v, 9.8 mM) and nickel(II) chloride hexahydrate (0.24% w/v, 10 mM, 1 eq.) and (b) a DMF solution of **1** (0.50% w/v, 9.8 mM) and copper(II) chloride dihydrate (0.34% w/v, 10 mM, 1 eq.).

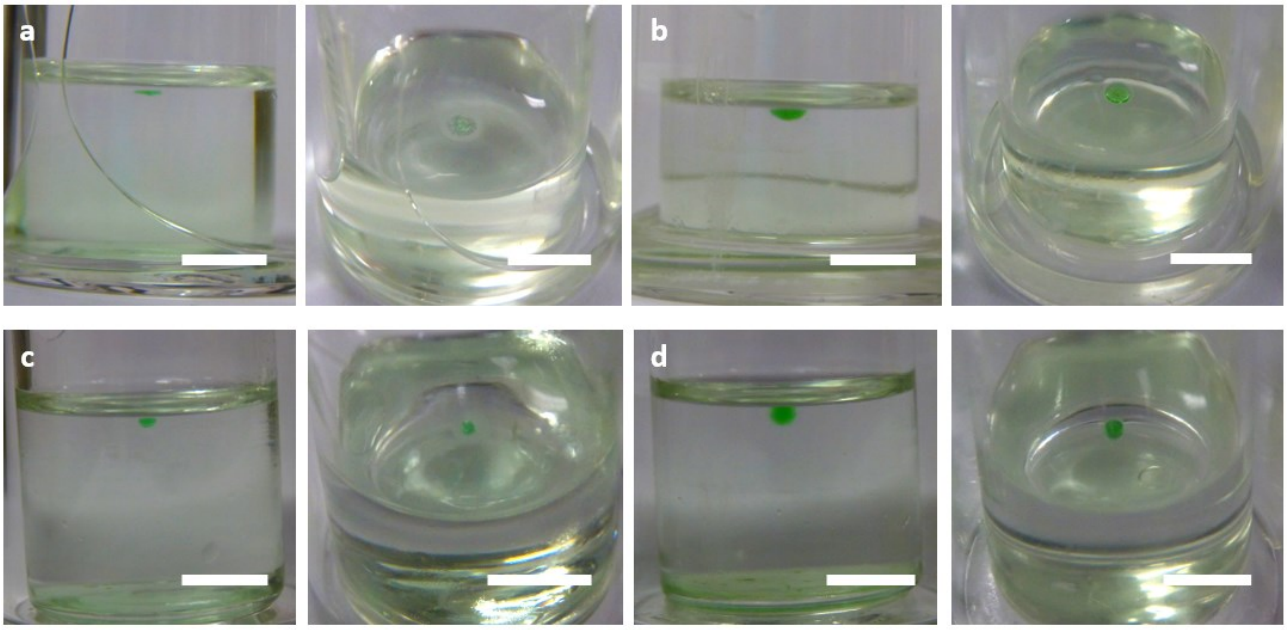

Fig. S14 Side and top-down views of lilypad aggregates formed at the room temperature by the diffusion of diethyl ether into (a) a 4.0 mM solution of **1** after 2 hours, (b) a 9.8 mM solution of **1** after 2 hours, (c) a 4.0 mM solution of **1** after 8 hours and (d) a 9.8 mM solution of **1** after 8 hours. All solutions contained an initial nickel(II) chloride hexahydrate concentration of 10 mM. Scale bars 5 mm.

4.2 Conformational analysis

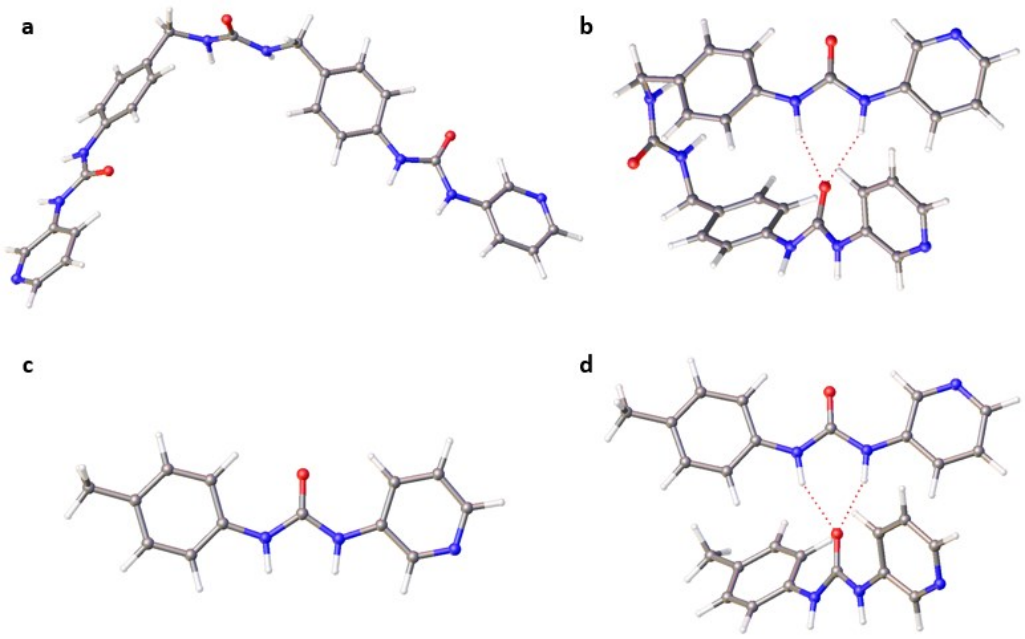

Fig. S15 Optimised geometries of **1** in its extended (a) and folded (b) conformations and **3** as a monomer (c) and hydrogen bonded dimer (d). Calculations were performed in Gaussian 16 with the B3LYP functional. The structures were initially optimised in the basis set 6-31+G* then refined in the larger basis set 6-31++G**. The optimised distances between the urea carbon atoms of structures (a), (b) and (d) are 13.158, 4.827 and 4.810 Å, respectively.

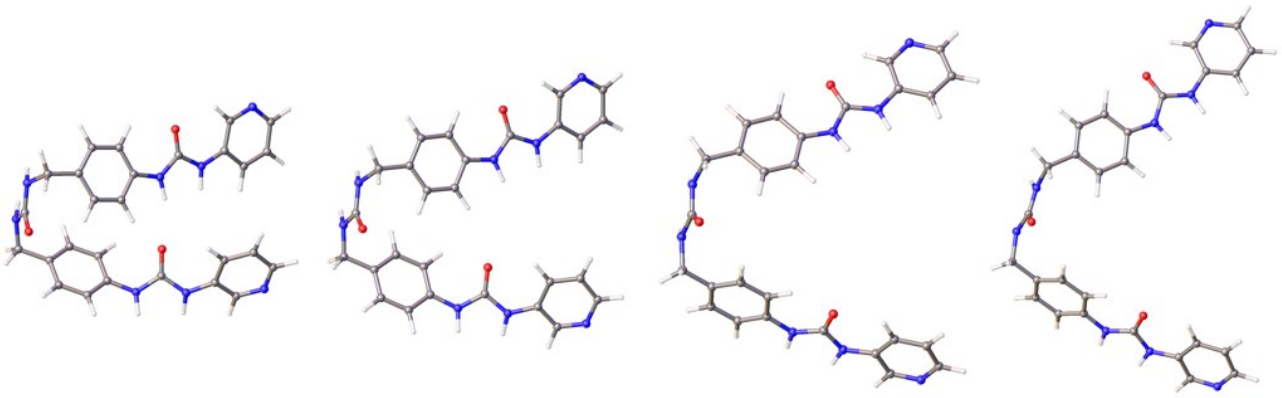

Fig. S16 Conformations adopted by **1** during intramolecular hydrogen bond formation, illustrating changes in the relative orientations of the benzyl and urea groups. Structures were calculated in the basis set 6-31+G* for a range of fixed urea-urea distances, $d_{urea-urea}$, measured between the carbonyl carbon atoms. The energy of each structure, ΔE, is expressed relative to the optimal folded conformation. As the highest-energy geometry identified in our conformational scan, the structure with $d_{urea-urea}$ = 7.3 Å is the estimated transition state for intramolecular hydrogen bonding.

Structure	Interaction energy / kJ mol^{-1}					
	6-31+G*	**6-31++G****	**aug-cc-pVDZ**	**def2-TZVP**	**Mean**	**Standard deviation**
Folded geometry of **1**	15.84	14.70 (-7.2%)	12.20 (-22.9%)	11.67 (-26.3%)	12.9 (-18.8%)	1.6
Dimer of **3**	34.63	34.73 (+0.3%)	32.27 (-6.8%)	30.66 (-11.5%)	32.6 (-6.0%)	2.0

Table S2 Interaction energies for the folded geometry of **1** and dimer of **3** in different basis sets. Percentage differences between the energies in 6-31+G* and larger basis sets 6-31++G**, aug-cc-pVDZ and def2-TZVP are given in brackets. Mean energies and their standard deviations are based on calculations in the larger basis sets.

5. Infrared spectroscopy

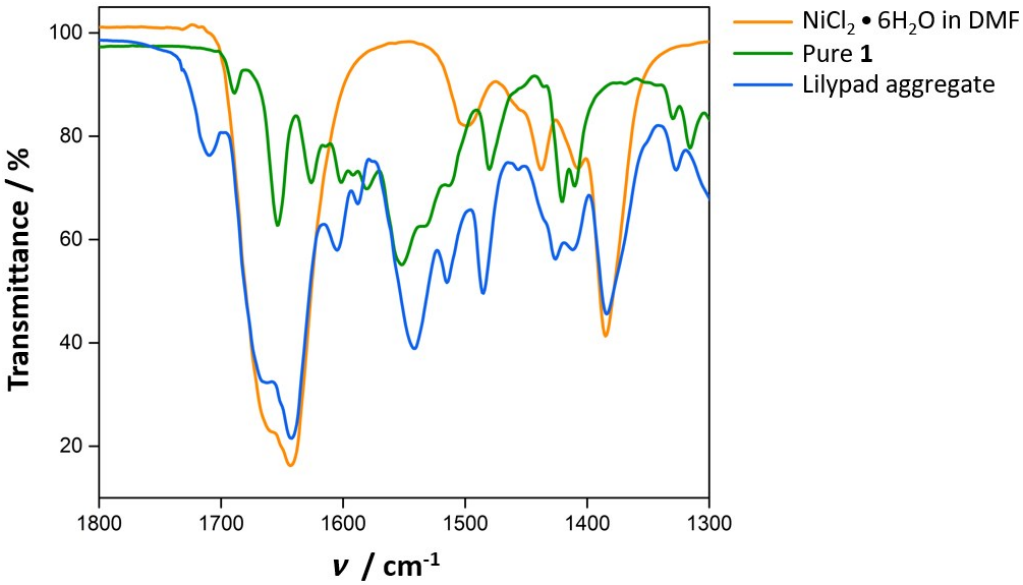

Fig. S17 FT-IR spectra of pure compound **1**, a dried lilypad aggregate prepared from **1** and nickel(II) chloride hexahydrate in DMF-ether, and an evaporated solution of nickel(II) chloride hexahydrate in DMF.

6. X-ray photoelectron spectroscopy

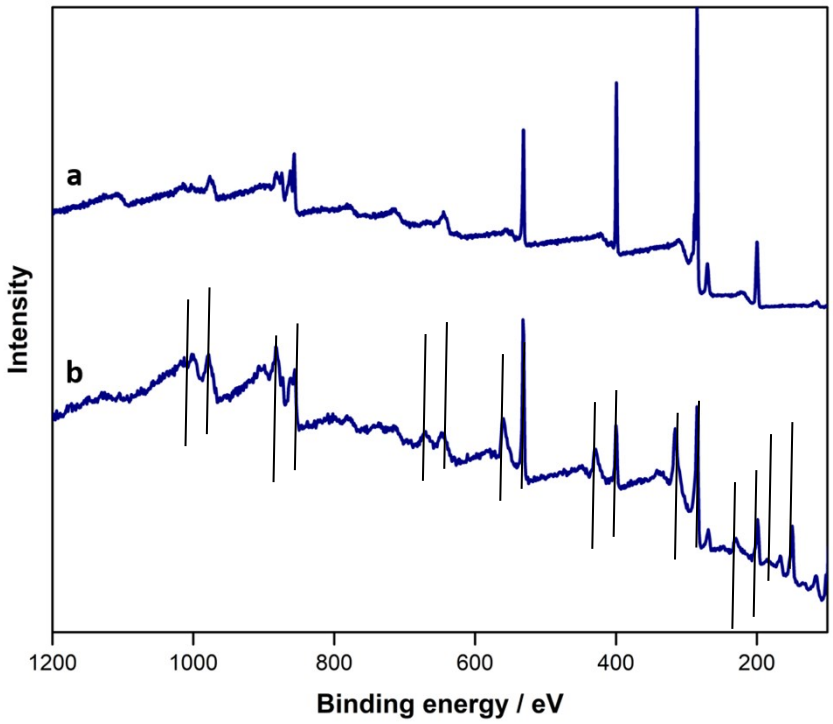

Fig. S18 Wide-scan XPS spectra for (a) a powdered equimolar mixture of **1** and nickel(II) chloride hexahydrate and (b) a vacuum-dried lilypad aggregate prepared from **1** and nickel(II) chloride hexahydrate in DMF-ether.

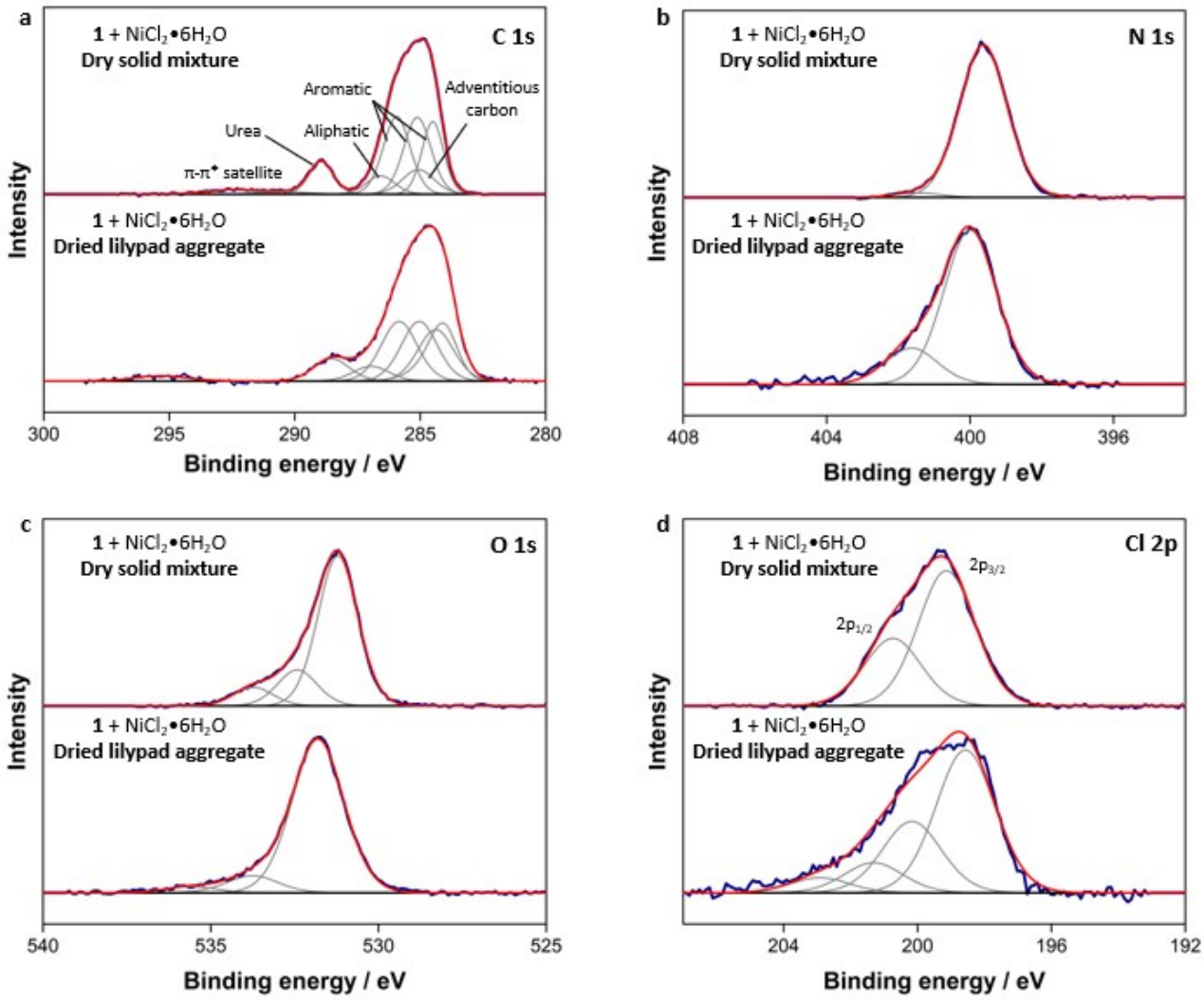

Fig. S19 Background-subtracted XPS spectra in the (a) C 1s, (b) N 1s, (c) O 1s and (d) Cl 2p regions for a powdered equimolar mixture of **1** and nickel(II) chloride hexahydrate and a vacuum-dried lilypad aggregate prepared from **1** and nickel(II) chloride hexahydrate in DMF-ether. Raw data are shown in blue, components in grey and envelope fits in red. Signals are fitted with symmetric *GL*(30) functions and energies calibrated against the sp^2 C 1s signal at 284.5 eV. For each element, all core signals other than the reference C 1s signal are fitted with equal full-width-at-half-maximum (FWHM) values.

7. Scanning electron microscopy

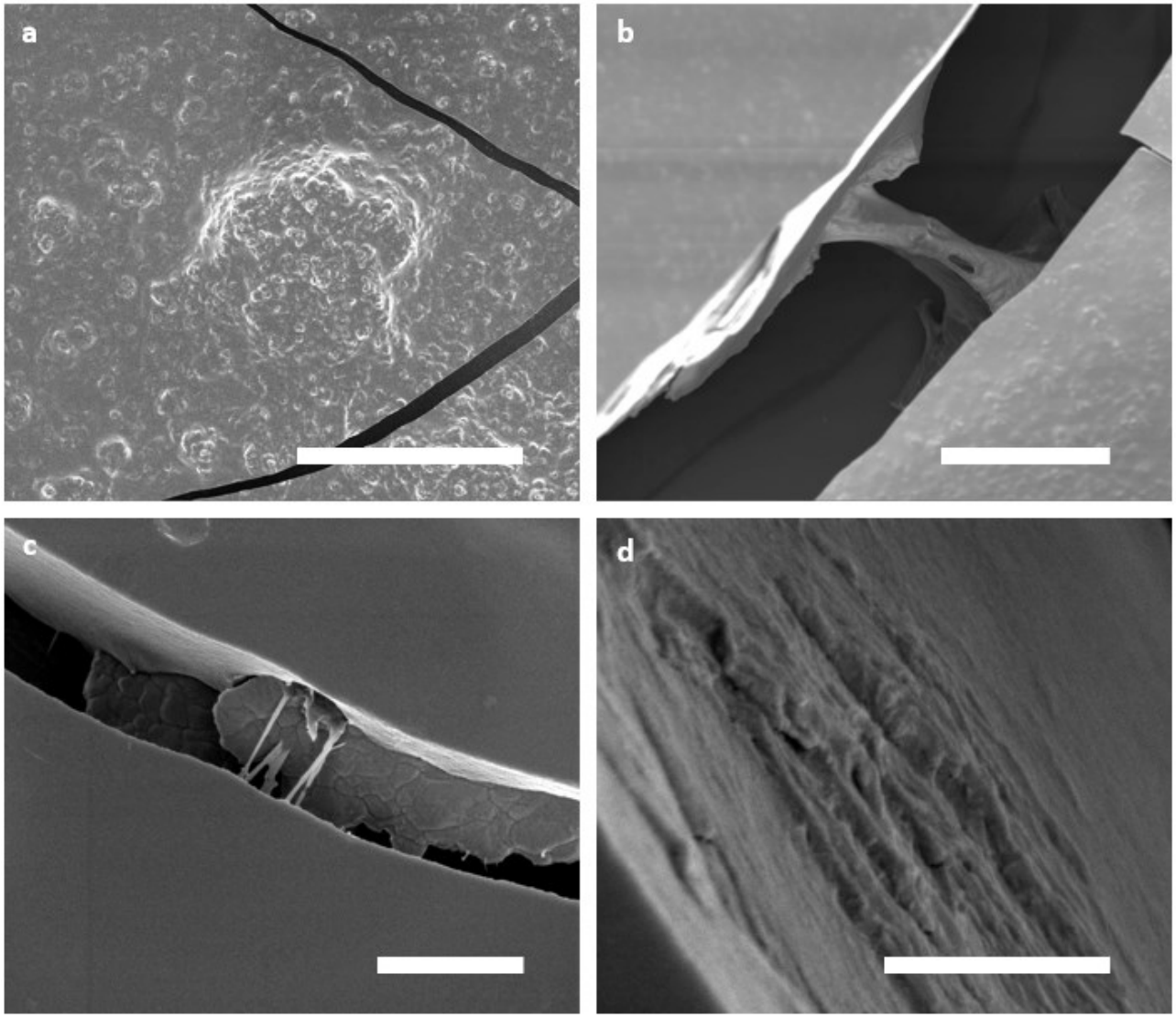

Fig. S20 SEM micrographs of lilypad aggregates after drying in air and coating with 2 nm platinum. Scale bars represent (a) 10 µm, (b) 5 µm, (c) 1 µm and (d) 500 nm.

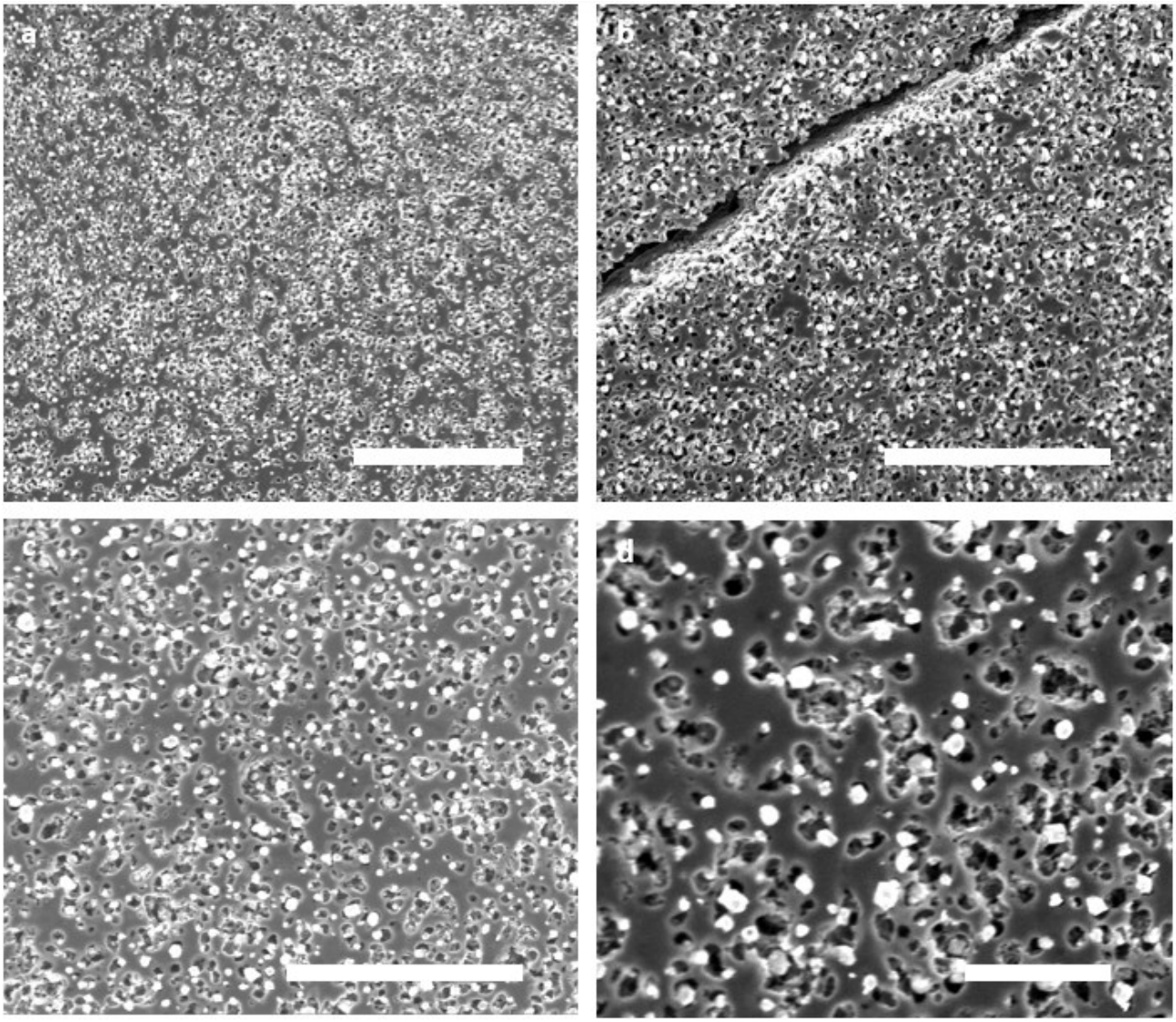

Fig. S21 SEM micrographs of uncoated lilypad aggregates after pyrolysis at 900 ^{o}C, at varying levels of magnification. Scale bars represent (a) 5 µm, (b) 4 µm, (c) 3 µm and (d) 1 µm.

8. Powder X-ray diffraction

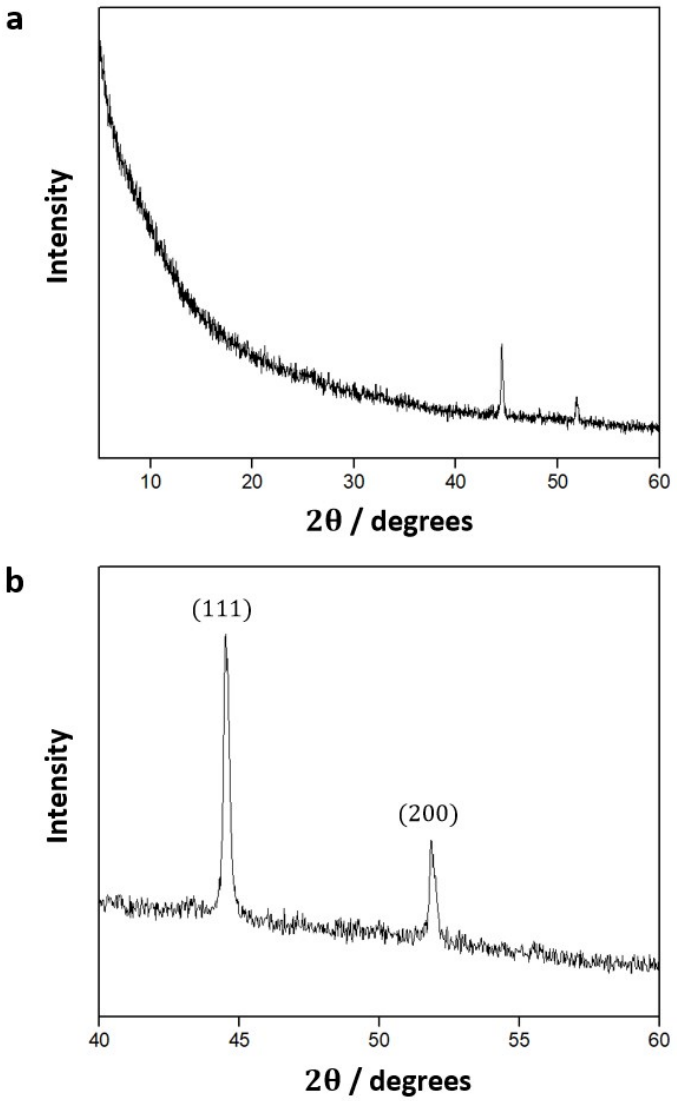

Fig. S22 PXRD data for a lilypad aggregate prepared from **1** and nickel(II) chloride hexahydrate in DMF-ether, after pyrolysis at 900°C: (a) data over a wide range of 2θ reveal an absence of reflections below 40°, suggesting no crystalline organic material is present; (b) peaks at 44.5 and 51.9° are correspond to the (111) and (200) reflections of elemental nickel.

9. Inductively coupled plasma mass spectrometry

Sample	Mass / µg	Ni loading / % w/w				Mean / % w/w	Ni absorbed from parent sol / %
		^{58}Ni	^{60}Ni	^{61}Ni	^{62}Ni		
Aggregate	778	5.36	5.42	5.40	5.29	5.37 ± 0.06	3.5
Pyrolysate	195	35.33	35.44	35.95	35.15	35.5 ± 0.3	5.9

Table S3 Estimated ICP-MS nickel loadings in a vacuum-dried lilypad aggregate and a pyrolysate generated by heating a lilypad aggregate to 900°C under nitrogen. Lilypad aggregates were harvested from solutions containing 4.8 mg (20 mmol) nickel(II) chloride hexahydrate, corresponding to 1.2 mg nickel. Values are given for the total nickel loadings extrapolated from quantification of single isotopes, calibrated against standards made from a 1000 ppm Ni reference solution (Romil). Errors are estimated from the standard deviation of measurements for different nickel isotopes.

Final aggregate geometry f_{end} R_{end} / mm V_{end} / mm^3	 0.50 ± 0.07 0.76 ± 0.06 1.55 ± 0.25
[Ni] / M Precursor sol Lilypad aggregate	 0.0101 ± 0.02 0.61 ± 0.18
Mass Ni in V_{end} / µg Precursor sol Lilypad aggregate	 0.92 ± 0.15 56 ± 14
[Ni] scaling due to aggregation	60 ± 18

Table S4 Mean geometries and compositions of lilypad aggregates and their precursor sols, illustrating the effect of aggregation on the local nickel concentration (A_r = 58.69 g mol^{-1}). The original nickel concentration is calculated for a solution of **1** (0.50% w/v, 9.8 mM) and nickel(II) chloride hexahydrate (0.24% w/v, 1 eq.) before the addition of diethyl ether, assuming a total volume of 2.00 cm^3 and mass error of ± 0.1 mg.